Aging Cell (2013) **12**, pp11–23 Doi: 10.1111/acel.12018

NMDA receptor dysfunction contributes to impaired brain-derived neurotrophic factor-induced facilitation of hippocampal synaptic transmission in a Tau transgenic model

Sylvie Burnouf,[1,2,3,4]* Alberto Martire,[5]* Maxime Derisbourg,[1,2$] Cyril Laurent,[1,2$] Karim Belarbi,[1,2,3] Antoine Leboucher,[1,2] Francisco J. Fernandez-Gomez,[1,2] Laetitia Troquier,[1,2] Sabiha Eddarkaoui,[1,2] Marie-Eve Grosjean,[1,2] Dominique Demeyer,[1,2] Anne Muhr-Tailleux,[1,6,7] Alain Buisson,[8] Nicolas Sergeant,[1,2,3] Malika Hamdane,[1,2] Sandrine Humez,[1,2] Patrizia Popoli,[5] Luc Buée[1,2,3] and David Blum[1,2,3]

[1]Université Lille-Nord de France, UDSL, F-59045 Lille Cedex, France
[2]Inserm U837, Jean-Pierre Aubert Research Centre, IMPRT, F-59000, Lille, France
[3]CMRR, CHRU-Lille, F-59000, Lille, France
[4]Present address: Max-Planck Institute für Biologie des Alterns/Max-Planck Institute for Biology of Ageing, Gleueler Strasse 50a, D-50931, Köln, Germany
[5]Department of Therapeutic Research and Medicine Evaluation, Istituto Superiore di Sanità, I-00161 Rome, Italy
[6]Inserm U1011, 1 rue du Professeur Calmette, F-59019 Lille, France
[7]Institut Pasteur de Lille, 1 rue du Professeur Calmette, F-59019 Lille, France
[8]Grenoble Institute Neurosciences, U836 INSERM, Université J. Fourier, 38042, Grenoble, France

Summary

While the spatiotemporal development of Tau pathology has been correlated with occurrence of cognitive deficits in Alzheimer's patients, mechanisms underlying these deficits remain unclear. Both brain-derived neurotrophic factor (BDNF) and its tyrosine kinase receptor TrkB play a critical role in hippocampus-dependent synaptic plasticity and memory. When applied on hippocampal slices, BDNF is able to enhance AMPA receptor-dependent hippocampal basal synaptic transmission through a mechanism involving TrkB and N-methyl-D-Aspartate receptors (NMDAR). Using THY-Tau22 transgenic mice, we demonstrated that hippocampal Tau pathology is associated with loss of synaptic enhancement normally induced by exogenous BDNF. This defective response was concomitant to significant memory impairments. We show here that loss of BDNF response was due to impaired NMDAR function. Indeed, we observed a significant reduction of NMDA-induced field excitatory postsynaptic potential depression in the hippocampus of Tau mice together with a reduced phosphorylation of NR2B at the Y1472, known to be critical for NMDAR function. Interestingly, we found that both NR2B and Src, one of the NR2B main kinases, interact with Tau and are mislocalized to the insoluble protein fraction rich in pathological Tau species. Defective response to BDNF was thus likely related to abnormal interaction of Src and NR2B with Tau in THY-Tau22 animals. These are the first data demonstrating a relationship between Tau pathology and synaptic effects of BDNF and supporting a contribution of defective BDNF response and impaired NMDAR function to the cognitive deficits associated with Tauopathies.

Key words: Alzheimer's Disease; brain-derived neurotrophic factor; hippocampus; NMDAR; NR2B; Src; Tau; transgenic mouse.

Introduction

Alzheimer's disease (AD) is a neurodegenerative disorder characterized by major memory impairments. Neuropathologically, AD is defined by the presence of neurofibrillary tangles (NFT) made up of intraneuronal fibrillar aggregates of hyper- and abnormally phosphorylated Tau proteins and the extracellular accumulation of Aβ peptides into amyloid plaques (Masters *et al.*, 1985; Sergeant *et al.*, 2008). NFT are observed early in life and increase during aging (Braak *et al.*, 2011). The spatiotemporal progression of NFT from the entorhinal cortex and the hippocampus to the isocortical areas has been shown correlated with cognitive deficits (Duyckaerts *et al.*, 1997), supporting a pivotal role for Tau pathology in AD-related memory impairments.

Brain-derived neurotrophic factor (BDNF) is highly expressed in the hippocampus (Hofer *et al.*, 1990) where it plays, through the activation of its cognate TrkB receptor, a critical role in synaptic plasticity processes underlying learning and memory (Minichiello, 2009). For instance, in animal models, spatial memory is enhanced in the Morris water maze (MWM) task following intrahippocampal administration of BDNF during pretraining (Cirulli *et al.*, 2004) and is impaired following infusion of anti-BDNF antibodies (Mu *et al.*, 1999) or genetic deletion of *Bdnf* or *Ntrk2/TrkB* (Minichiello *et al.*, 1999; Heldt *et al.*, 2007). In addition, stimulation of spatial memory using the MWM task promotes an increase in hippocampal BDNF mRNA expression (Kesslak *et al.*, 1998). BDNF thus plays a crucial role in mechanisms underlying hippocampus-dependent memory.

Brain-derived neurotrophic factor mRNA and protein levels are reduced in the cortex and hippocampus of AD patients (for review see Schindowski *et al.*, 2008). So far, these alterations have been ascribed to a toxic effect of Aβ peptides. Indeed, *in vitro* and *in vivo* experimental studies demonstrate that Aβ accumulation is correlated with the decrease in BDNF expression (Garzon & Fahnestock, 2007; Peng *et al.*, 2009). Further, Aβ oligomers are able to impair BDNF retrograde axonal transport in Tg2576 primary neurons (Poon *et al.*, 2011), to specifically down-regulate BDNF transcripts IV and V in differentiated neuroblastoma cells (Garzon & Fahnestock, 2007) and to inhibit the proteolytic conversion of proBDNF to mature BDNF (Zheng *et al.*, 2010). Thus, memory alterations seen in AD could at least in part be related to an Aβ-induced loss of BDNF expression. In agreement, both the increase in

Correspondence
Dr. David Blum, Inserm U837, 'Alzheimer and Tauopathies', Place de Verdun, Lille Cedex 59045, France. Tel.: +33320298858; fax: +33320538562; e-mail: david.blum@inserm.fr

*First co-authors equally contributed to the work.
$Second co-authors equally contributed to the work.

Accepted for publication *20 September 2012*

© 2012 The Authors
Aging Cell © 2012 Blackwell Publishing Ltd/Anatomical Society of Great Britain and Ireland

Aging Cell

brain BDNF and the activation of TrkB receptors through small-molecule agonists can prevent the development of spatial memory deficits in experimental models mimicking the amyloid side of AD (Blurton-Jones *et al.*, 2009; Nagahara *et al.*, 2009).

Conversely, relationships between Tau pathology, which occurs early during the normal process of aging (Braak *et al.*, 2011), and BDNF expression and function are far less understood. Recently, we reported the absence of BDNF mRNA and protein down-regulation in a Tau transgenic mouse model – the THY-Tau22 model – (Burnouf *et al.*, 2012), which exhibits AD-like hippocampal Tau pathology paralleling hippocampus-dependent memory impairments (Schindowski *et al.*, 2006; Belarbi *et al.*, 2011; Van der Jeugd *et al.*, 2011). However, as hyperphosphorylated Tau species are relocalized to the somatodendritic compartment in AD and Tau transgenic mice (Schindowski *et al.*, 2006; Ballatore *et al.*, 2007; Hoover *et al.*, 2010; Ittner *et al.*, 2010), it remains uncertain whether beyond its basal expression, synaptic effects mediated by BDNF would be affected. Recent studies using slice electrophysiology demonstrated that perfusion of exogenous BDNF at a high rate induced a long-lasting enhancement of AMPAR-dependent basal synaptic transmission in hippocampal slices from adult rats or mice (Diogenes *et al.*, 2007; Tebano *et al.*, 2008; Ji *et al.*, 2010). This enhancement has been shown dependent on both TrkB and NMDAR (Diogenes *et al.*, 2007). In the present study, we have evaluated whether and how Tau pathology could impact on the effects of BDNF upon basal synaptic transmission in the THY-Tau22 transgenic mouse model.

Results

BDNF enhances hippocampal synaptic transmission in slices from adult mice

In a first attempt, we assessed the ability of exogenous BDNF application to enhance basal synaptic transmission, that is, to induce a long-lasting increase in AMPAR-dependent fEPSP, in the CA1 region of the hippocampus from 7-month-old (7-mo) WT mice. Constant-intensity stimuli were applied to CA3 Schaffer collateral fibers, giving rise to fEPSPs in the CA1 region. Once the fEPSP slope was stabilized, BDNF (10 ng mL^{-1}, 30 min, 156 mL h^{-1}) was added to the superfusion medium. As expected (Diogenes *et al.*, 2007; Tebano *et al.*, 2008; Ji *et al.*, 2010), this led to an increase in CA1 fEPSP slope reaching 130.2 ± 6.8% of baseline (last 5 min of BDNF application; $P = 0.0008$, $n = 9$; Fig. 1A and B). Noteworthy, BDNF effect was maintained even after BDNF washout. Then, we tested the effect of an inhibitor of Trk receptor autophosphorylation, K252a, on the ability of exogenous BDNF to enhance basal synaptic transmission. K252a was used at a concentration (200 nM) known to prevent BDNF action on hippocampal synaptic transmission but devoid of effect upon basal electrical activity (Tebano *et al.*, 2008). While application of K252a (200 nM; 40 min) did not by itself exert an effect on basal synaptic transmission in our conditions (95.5 ± 2.4% of baseline; $P = 0.4$; $n = 3$; Fig. 1B), it completely blocked exogenous BDNF-induced synaptic enhancement in WT mice (WT + BDNF: 130.2 ± 6.8% of baseline, $P = 0.0008$, $n = 9$; WT + BDNF + K252a: 105.5 ± 5.5% of baseline; $P = 0.0364$ vs. WT + BDNF; Fig. 1A and B). In addition, application of the selective noncompetitive N-methyl-D-Aspartate receptors (NMDAR) antagonist MK801 (20 μM; 40 min) abolished BDNF-induced synaptic facilitation in WT mice (BDNF: 134.6 ± 5.5% of baseline, $P = 0.011$; BDNF + MK801: 106.7 ± 7.7% of baseline, $P = 0.268$, $n = 4$–5; Fig. 1C), in line with previous observations in rat (Diogenes *et al.*, 2007). MK801 alone did not modify AMPAR-dependent basal synaptic transmission (Fig. 1D). Ifenprodil (5 μM; 40 min), a specific blocker of the NR2B subunit of NMDAR, similarly abolished the increase in the fEPSP slope induced by BDNF (Fig. 1E and F) supporting a need for NR2B subunit in the ability of BDNF to enhance synaptic transmission. Collectively, these data indicate that exogenous BDNF application induces an increase in AMPAR-dependent basal synaptic activity that requires activation of both TrkB and NMDAR.

Loss of BDNF-induced synaptic enhancement is concomitant to hippocampal Tau pathology and memory impairments in THY-Tau22 mice

We then evaluated the effects of exogenous BDNF on synaptic efficacy in THY-Tau22 mice at the age of 7 months. At this time point, THY-Tau22 animals displayed hyperphosphorylated Tau in the CA1 region of the hippocampus as observed using immunohistochemistry (Fig. 2A, upper panel) and western blotting (Fig. 2A, lower panel). Interestingly, hyperphosphorylated Tau species were observed in the somatodendritic compartment of hippocampal neurons (Fig. 2B, upper panel) and more particularly in a synaptic subfraction exhibiting the biochemical characteristics of postsynaptic densities (PSD), that is, enriched in PSD95 and sparse in Syntaxin1 (PSD vs. non-PSD; Fig. 2B, lower panel). Levels of PSD95 and Syntaxin1 were similar between WT and THY-Tau22 mice ($n = 5$ per group; NS) supporting lack of synaptic loss and neuronal death at this stage, as previously suggested (Van der Jeugd *et al.*, 2011). The presence of Tau pathology was found correlated with deficits in spatial learning and memory abilities in the MWM task (Fig. 2C). Indeed, during the learning phase of the test, THY-Tau22 animals exhibited an increased escape latency as compared with WT mice [$F_{(1,88)} = 11.80$, $P < 0.001$; Fig. 2C, left panel] albeit velocity did not differ between groups (WT: 9.93 ± 0.47 cm s^{-1} vs. THY-Tau22: 9.95 ± 0.52 cm s^{-1}; $n = 12$ per group; NS). In the probe phase, WT mice spent significantly more time in the target quadrant than in the others ($P = 0.044$; Fig. 2C, right panel), while mutants showed no preference ($P = 0.25$). To evaluate whether these pathological features could be associated with changes in BDNF effects upon basal synaptic transmission, we assessed the ability of BDNF to increase fEPSP in THY-Tau22 mice hippocampus. Strikingly, while BDNF application (10 ng mL^{-1}, 30 min, 156 mL h^{-1}) led to an increase in 120.3 ± 5.3% of basal CA1 fEPSP slope in 7-mo WT slices (last 5 min of BDNF application; $P = 0.041$, $n = 13$; Fig. 2D), no BDNF-induced synaptic enhancement was observed in slices from littermate THY-Tau22 mice (94.5 ± 1.6% of baseline; $P > 0.05$; $n = 8$; Fig. 2D). Instead, BDNF application induced a slight but significant decrease in fEPSP slope in THY-Tau22 hippocampal slices (88.7 ± 2.9% of baseline after 10 min of treatment; $P = 0.015$ vs. THY-Tau22 baseline; $n = 8$; Fig. 2D; noted as on Fig. 2D). Lack of BDNF-induced synaptic enhancement observed in THY-Tau22 mice was unrelated to changes in AMPAR-dependent basal synaptic transmission because the I/O curve remained similar between WT and THY-Tau22 mice (Fig. 2E). Altogether, our data indicate that while basal AMPAR-dependent synaptic transmission remained unaltered in THY-Tau22 mice, Tau pathology and memory impairments were associated with a defect in the ability of BDNF to increase synaptic efficacy. As both TrkB and NMDAR are involved in the induction of BDNF effect (see Fig. 1 and Diogenes *et al.*, 2007), we next evaluated their respective functionality in THY-Tau22 mice.

TrkB activatability in THY-Tau22 mice

As a first step, the expressions of full-length TrkB (TrkB-FL) receptors and its truncated dominant-negative form (TrkB-T1) were evaluated by

© 2012 The Authors
Aging Cell © 2012 Blackwell Publishing Ltd/Anatomical Society of Great Britain and Ireland

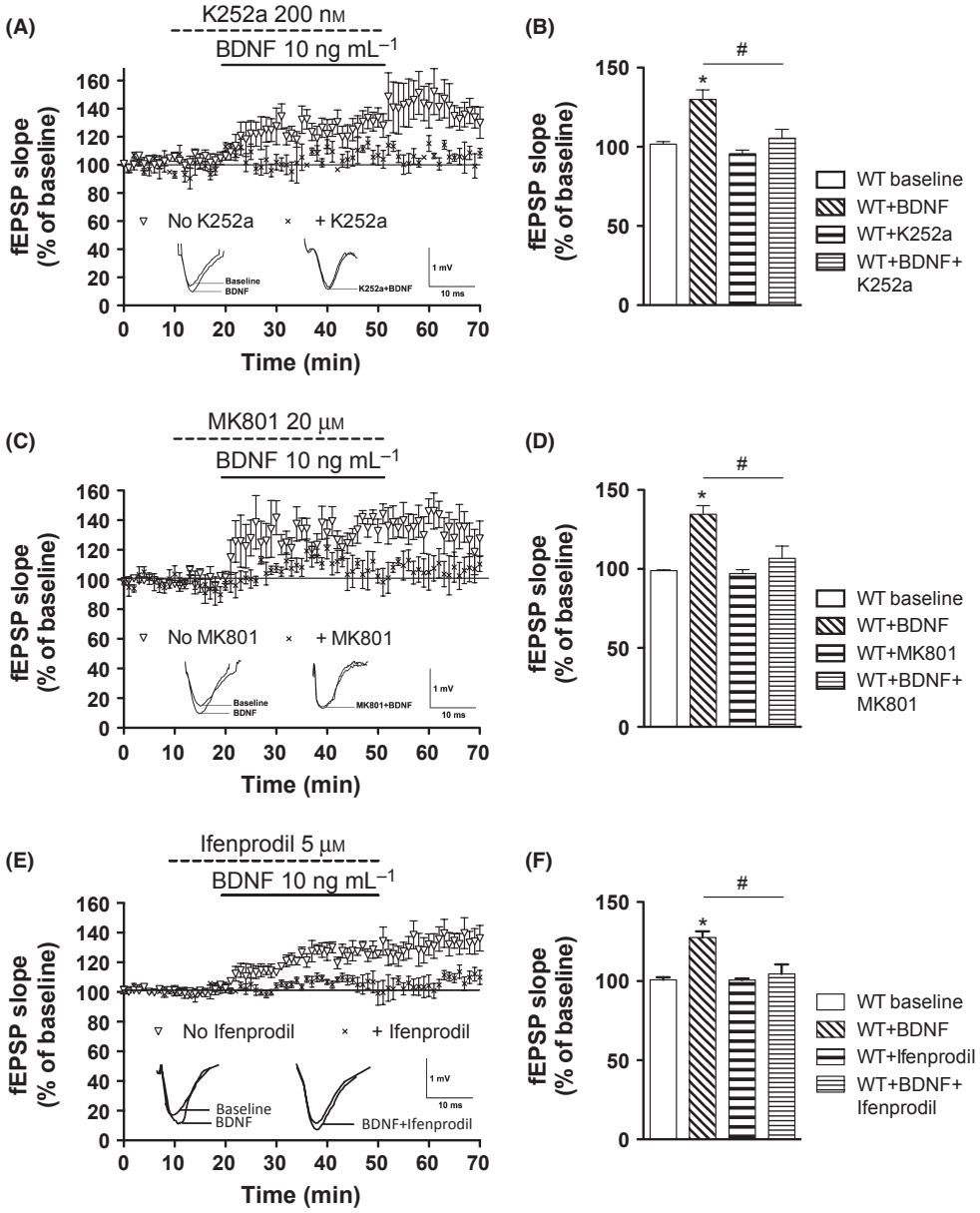

Fig. 1 Brain-derived neurotrophic factor (BDNF)-induced enhancement of hippocampal synaptic transmission in WT mice is TrkB and NMDAR dependent. (A) In WT mice, BDNF application (10 ng mL^{-1}, 30 min) induces a long-term enhancement of synaptic transmission completely abolished by the co-application of the tyrosine kinase inhibitor K252a (200 nM, 40 min). Insets show representative fEPSP recordings demonstrating the BDNF effect in the presence or absence of K252a. Calibration bars: 1 mV, 10 ms. Periods of drug application are indicated by horizontal bars. (B) Representative histogram of fEPSP slope variation during the last 5 min of BDNF and/or K252a application expressed as the mean percentage of baseline, in hippocampal slices from WT mice. $n = 3$–9 per group. (C) In WT mice, BDNF application (10 ng mL^{-1}, 30 min) induces a long-term enhancement of synaptic transmission completely abolished by the co-application of the NMDAR antagonist MK801 (20 µM, 40 min). Insets show representative fEPSP recordings demonstrating the BDNF effect in the presence or absence of MK801. Calibration bars: 1 mV, 10 ms. Periods of drug application are indicated by horizontal bars. (D) Representative histogram of fEPSP slope variation during the last 5 min of BDNF and/or MK801 application expressed as the mean percentage of baseline, in WT hippocampal slices. $n = 4$–5 per group. *$P < 0.05$ WT + BDNF vs. WT baseline, #$P < 0.05$ vs. WT + BDNF. Neither K252a (B) nor MK801 (D) modified the fEPSP slope on their own in WT hippocampal slices. (E) In WT mice, BDNF application (10 ng mL^{-1}, 30 min) induces a long-term enhancement of synaptic transmission completely abolished by the co-application of the NR2B inhibitor Ifenprodil (5 µM, 40 min). Insets show representative fEPSP recordings demonstrating the BDNF effect in the presence or absence of Ifenprodil. Calibration bars: 1 mV, 10 ms. Periods of drug application are indicated by horizontal bars. (F) Representative histogram of fEPSP slope variation during the last 5 min of BDNF and/or Ifenprodil application expressed as the mean percentage of baseline, in hippocampal slices from WT mice. $n = 4$ per group. *$P < 0.05$ WT + BDNF vs. WT baseline, #$P < 0.05$ WT + BDNF + Ifenprodil vs. WT + BDNF. Ifenprodil did not modify the fEPSP slope on its own in WT hippocampal slices.

western blotting. Both TrkB-FL and TrkB-T1 expressions remained unchanged in the hippocampus of 7-mo THY-Tau22 mice as compared with WT mice (Fig. 3A). In line, hippocampal mRNA expression of TrkB remained unchanged in Tau transgenic mice (112.0 ± 5.4% of WT, $P > 0.05$). We also evaluated expression of the p75 receptor whose activation by proBDNF is prone to impact hippocampal synaptic transmission (Woo *et al.*, 2005; Martinowich *et al.*, 2012). While p75 mRNA was found significantly upregulated in Tau mice hippocampus

© 2012 The Authors
Aging Cell © 2012 Blackwell Publishing Ltd/Anatomical Society of Great Britain and Ireland

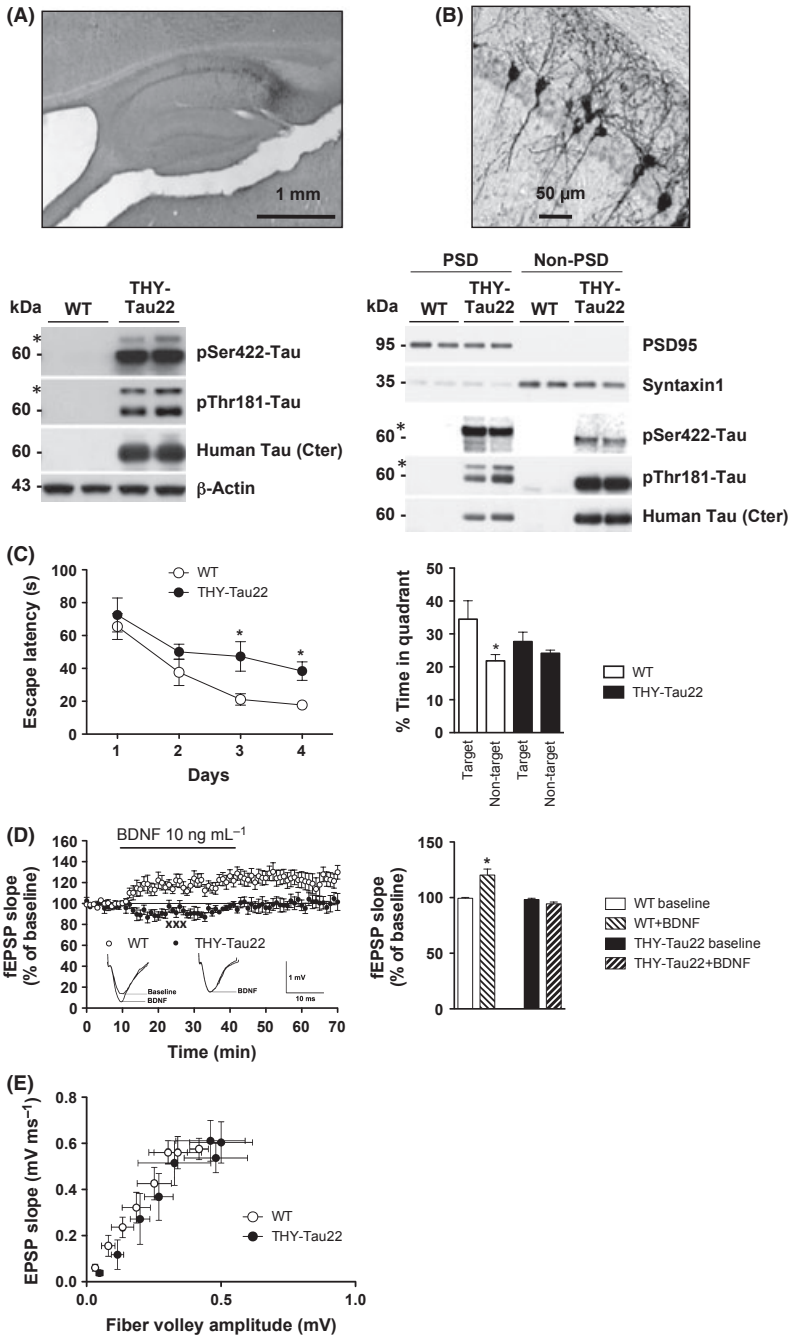

Fig. 2 Synaptic Tau pathology, cognitive impairments, and loss of brain-derived neurotrophic factor (BDNF)-induced enhancement of hippocampal synaptic transmission in THY-Tau22 mice. (A) Top: immunohistochemical labeling of the pathological pThr212/Ser214 (AT100) Tau epitope in hippocampal sagittal section from 7-mo THY-Tau22 mice (scale bar = 1 mm). Bottom: western blot analysis from hippocampal homogenates of 7-mo mice shows Tau pathology in THY-Tau22 mice, using the pSer422 and pThr181 Tau epitopes. The most hyperphosphorylated Tau species are shifted to a higher apparent molecular weight (*). Total human Tau was labeled with the anti-Tau C ter antibody. None of these staining was observed in WT animals. β-actin was used as an internal loading control. (B) Top: pathological Tau species display a somatodendritic localization within CA1 neurons of THY-Tau22 mice, as assessed using the AT100 antibody (scale bar = 50 µm). Bottom: apparent molecular weight of Tau was found increased in postsynaptic densities (PSD) fractions of 7-mo THY-Tau22 mice (*) signing that most phosphorylated Tau species localize in these fractions vs. non-PSD fractions. No staining was observed in age-matched WT mice. $n = 5$ per group. (C) THY-Tau22 mice show defects in the Morris water maze learning (left panel) and memory (right panel) task at the age of 7-mo. $n = 12$ per group. *$P < 0.05$. (D) Left panel: BDNF application (10 ng mL^{-1}, 30 min) fails to induce a long-lasting enhancement of synaptic transmission in hippocampal slices from 7-mo THY-Tau22 mice. Insets show representative fEPSP recordings in WT and THY-Tau22 mice, before (baseline) and 30 min after BDNF application. Each trace is the average of three successive fEPSPs (stimulation artefacts have been truncated). Calibration bars: 1 mV, 10 ms. The period of drug application is indicated by the horizontal bar. Right panel: representative histograms of fEPSP slope variation during the last 5 min of BDNF application, expressed as the mean percentage of baseline, in hippocampal slices from 7-mo WT and THY-Tau22 mice. $n = 8$–13 per group. *$P < 0.05$ WT + BDNF vs. WT baseline. In THY-Tau22 mice, during BDNF application, a slight but significant decrease of fEPSP slope (after 10 min of treatment $P < 0.05$ vs. THY-Tau22 baseline; $n = 8$) was observed (indicated by xxx). (E) Input/output curves, displayed as the relationship between fEPSP slope (ordinates) and the amplitude of the presynaptic volley (abscissa), show no change in basal synaptic transmission in 7-mo THY-Tau22 mice as compared with WT animals. For each group, the data are mean ± SEM (for both fiber volley and fEPSP slope in each data point). $n = 3$–5 per group. $P > 0.05$ vs. WT.

© 2012 The Authors
Aging Cell © 2012 Blackwell Publishing Ltd/Anatomical Society of Great Britain and Ireland

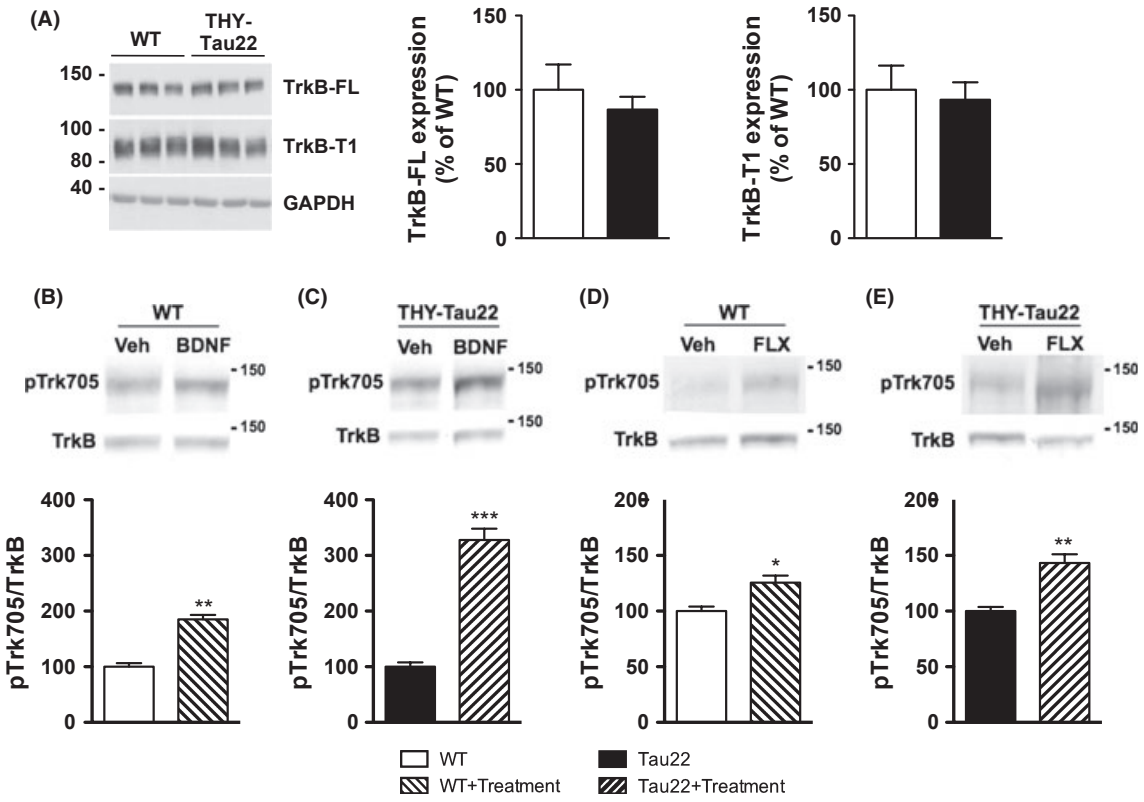

Fig. 3 Protein expression and *in vivo* activation of TrkB receptor in THY-Tau22 mice. (A) Representative western blot (left) and quantifications (right) of full-length (TrkB-FL) and truncated (TrkB-T1) TrkB receptor protein expression in the hippocampus of 7-mo WT and THY-Tau22 mice. n = 5–8 per group. $P > 0.05$ vs. WT. GAPDH was used as an internal loading control. (B–E) TrkB activation is induced by intrahippocampal stereotaxic injection of brain-derived neurotrophic factor (B–C; 100 ng in 2 μL, 0.25 μL min^{-1}) or intraperitoneal injection of fluoxetine (D–E; 30 mg kg^{-1}). Phosphorylation of TrkB at Y705 is visualized following lectin precipitation and western blotting. Both types of stimulation induced TrkB autophosphorylation at Y705 in its catalytic domain in the hippocampus of 7-mo WT (C and E) and THY-Tau22 (D and F) mice. n = 3–4 per group. *$P < 0.05$ vs. WT, **$P < 0.01$ vs. WT, *** $P < 0.001$ vs. WT.

(174.8 ± 14.3% of WT, $P = 0.012$ using Student's t-test; Fig. S1A), we found no change at the protein level ($P > 0.05$; Fig. S1B).

Using Y705 phosphorylation (pTrk705) as an activation index, we evaluated basal TrkB phosphorylation as well as the *in vivo* ability of TrkB to be activated following two different activation paradigms: the stereotaxic intra-CA1 injection of BDNF (100 ng) and intraperitoneal injection of the antidepressant Fluoxetine (FLX-HCl; 30 mg kg^{-1}; Rantamaki *et al.*, 2007; Allaman *et al.*, 2011). In basal conditions, we observed that the pTrk705/TrkB ratio was significantly increased by 60.9 ± 7.3% in the hippocampus of untreated THY-Tau22 mice (Fig. 3B vs. C and D vs. E; $P = 0.0002$ vs. WT littermates, using Student's t-test; n = 3–4; data not shown). Further, we observed that BDNF injection enhanced TrkB phosphorylation at Y705 in the hippocampus of WT (185.1 ± 8.2% vs. saline, $P = 0.0013$, $n = 4$, Fig. 3B) and THY-Tau22 mice (327.9 ± 20.1% vs. saline, $P = 0.0005$, $n = 4$, Fig. 3C). Similar results were obtained following the intraperitoneal injection of FLX-HCl in WT (125.5 ± 6.3% vs. saline, $P = 0.027$; n = 3–4) and THY-Tau22 (143.2 ± 7.8% vs. saline, $P = 0.008$; n = 3–4) animals (Fig. 3D and E).

As cholesterol in lipid rafts is crucial for TrkB activation (Suzuki *et al.*, 2004; Assaife-Lopes *et al.*, 2010), we quantified cholesterol concentration in lipid raft fractions (GM1-enriched; Fig. S2B) from 7-mo WT and THY-Tau22 mice and found no difference between the two groups (Fig. S2A; $P = 0.48$; $n = 4$). In addition, we found no difference in TrkB distribution within lipid raft fractions between WT and THY-Tau22 mice (Fig. S2B). Finally, we also examined whether THY-Tau22 mice exhibited changes in PLCγ, a component of TrkB downstream signaling that is involved in synaptic signaling promoted by BDNF (see Minichiello, 2009 for review). As shown on Fig. S3A, we observed neither a change in PLCγ expression nor in its activation status (Y783 phosphorylation). Finally, as PLCγ interacts with Tau proteins (Reynolds *et al.*, 2008), we evaluated its distribution between sarkosyl-soluble and insoluble fractions because a potential modification of its solubility would likely be indicative of a modified function. As shown on Fig. S3B, while hyperphosphorylated and aggregated pathological Tau species were recovered in the sarkosyl-insoluble protein fraction – as indicated by the detection of abnormal phosphorylation using AT100 and AP422 antibodies – PLCγ strictly remained in the sarkosyl-soluble fraction in both WT and THY-Tau22 mice hippocampus.

Altogether, these observations support the view that the lack of BDNF-induced synaptic enhancement is unrelated to impaired TrkB function and suggest alterations downstream of TrkB receptor, possibly involving NMDAR dysfunction.

Impairment of NMDAR activatability and NR2B subunit in THY-Tau22 mice

Next, we evaluated the activatability of NMDAR in the hippocampus of 7-mo WT and THY-Tau22 mice by exposing hippocampal slices to a specific agonist of NMDAR, that is, the NMDA, of which direct application is known to induce fEPSP depression as a consequence of strong calcium entry and strong depolarization of the postsynaptic

© 2012 The Authors
Aging Cell © 2012 Blackwell Publishing Ltd/Anatomical Society of Great Britain and Ireland

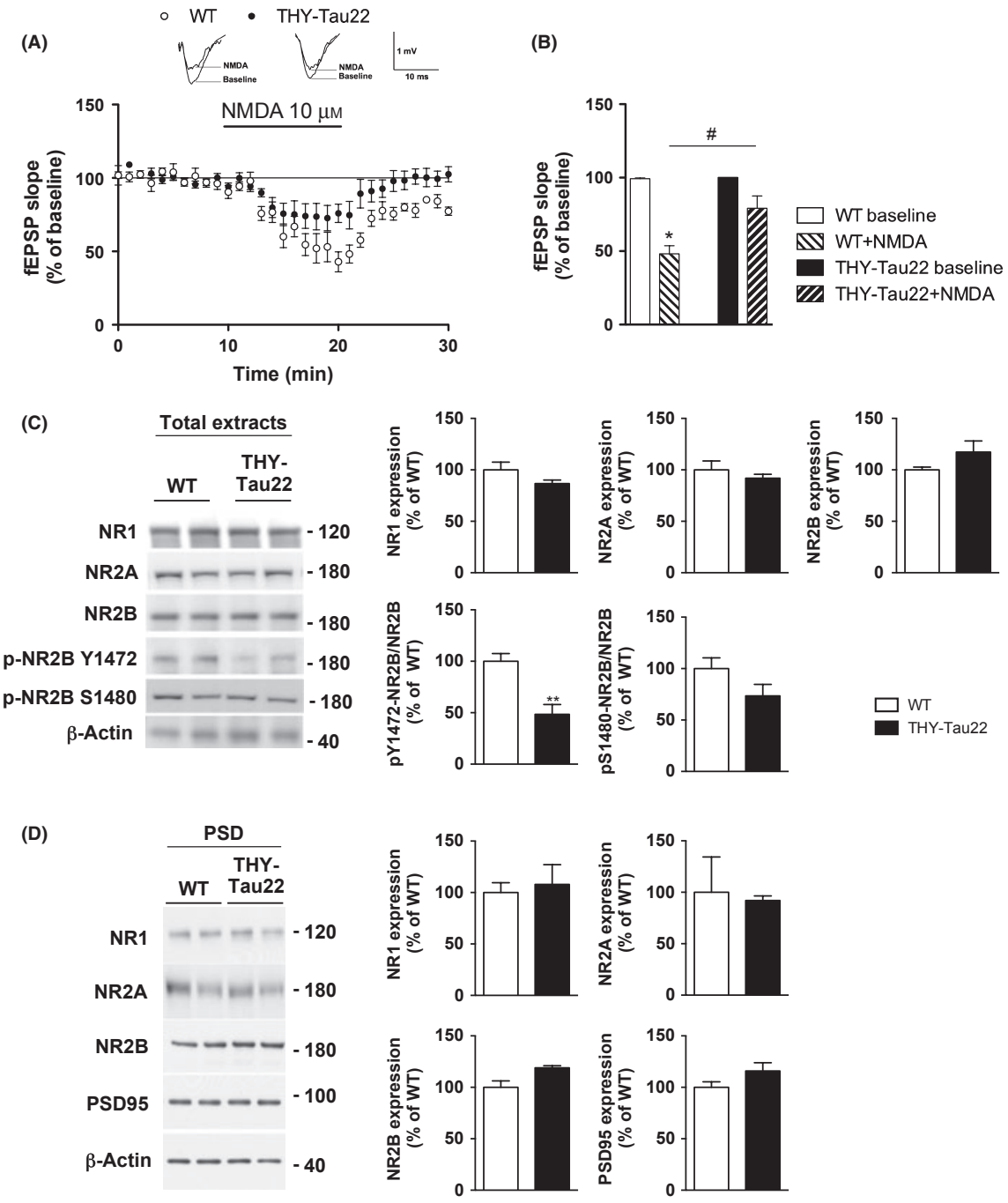

Fig. 4 Impaired NMDAR function in the hippocampus of THY-Tau22 mice. (A) NMDAR activation is visualized following direct NMDA application (10 µM, 10 min) and characterized in hippocampal slices from 7-mo WT animals by a transient depression of fEPSPs. The response to NMDA activation is impaired in age-matched THY-Tau22 mice as compared with WT animals. Insets show representative fEPSP recordings in WT and THY-Tau22 mice, before (baseline) and 10 min after NMDA application. Calibration bars: 1 mV, 10 ms. The period of drug application is indicated by the horizontal bar. (B) Representative histogram of fEPSP slope variation during the last 5 min of NMDA application, expressed as the mean percentage of baseline. $n = 5$–7 per group. *$P < 0.05$ WT + NMDA vs. WT baseline. #$P < 0.05$ THY-Tau22 + NMDA vs. WT + NMDA. (C) Expression of NMDAR subunits and phosphorylated forms of NR2B subunit in total protein extracts from 7-mo THY-Tau22 mice and littermate WT animals. Quantifications are given on the right panel. **$P < 0.001$ vs. WT. (D) Expression of NMDAR subunits in postsynaptic densities fractions from 7-mo THY-Tau22 mice and WT littermates. Quantifications are given on the right panel.

membrane (Mallon *et al.*, 2005). As extensively shown in both corticostriatal (Domenici *et al.*, 2003) and hippocampal slices (Tebano *et al.*, 2005), this electrophysiology protocol allows the evaluation of the level of NMDAR activation and its modulation in different conditions. As shown in Fig. 4A and B, direct NMDA application on hippocampal slices (10 µM, 10 min) induced a reversible depression of the fEPSP slope (−51.8 ± 5.5% of baseline; $P = 0.008$; $n = 5$) in WT mice. This effect was significantly attenuated in THY-Tau22 mice (−20.9 ± 8.4% of baseline, $P = 0.16$; $n = 7$; WT + NMDA vs. THY-Tau22 + NMDA: $P = 0.03$).

© 2012 The Authors
Aging Cell © 2012 Blackwell Publishing Ltd/Anatomical Society of Great Britain and Ireland

Decreased NMDA effect was not associated with impairments of global NMDAR subunits expressions. Indeed, we observed no difference in hippocampal NR2A and NR2B mRNA expressions (not shown) nor in NR1, NR2A, and NR2B protein levels in both total protein extracts and PSD fractions (n = 5–6 per group; NS vs. WT littermates; Fig. 4C and D) nor in NR2A/NR2B ratio (WT: 0.53 ± 0.05; THY-Tau22: 0.46 ± 0.03; NS using Student's t-test) between 7-mo THY-Tau22 mice and WT littermates. However, we observed a significant decrease in NR2B phosphorylation at Y1472, a critical site for NMDAR synaptic signaling, in THY-Tau22 mice (−51.5 ± 4.4% vs. WT, P = 0.0012; n = 6; Fig. 4C). Phosphorylation of NR2B at Ser1480 by Casein Kinase 2 (CK2) has recently been suggested to promote dephosphorylation of NR2B at Y1472 epitope (Sanz-Clemente *et al.*, 2010). We thus evaluated NR2B phosphorylation at Ser1480 as well as CK2 status in the hippocampus of THY-Tau22 mice. As shown on Fig. 4C, NR2B phosphorylation at Ser1480 was found comparable in WT littermates and THY-Tau22 mice. Also, neither total CK2 expression nor distribution in sarkosyl-soluble and insoluble protein fractions were found modified in Tau transgenic mice (Fig. 5A and B).

Then, we analyzed the two main non-receptor tyrosine kinases known to directly phosphorylate NR2B at Y1472: Fyn and Src (Prybylowski *et al.*, 2005; Xu *et al.*, 2006; Zhang *et al.*, 2008). While Src phosphorylates NR2B independently of BDNF/TrkB pathway, Fyn kinase is required for the increase in NMDAR activity elicited by BDNF and is thus involved in the crosstalk between TrkB and NMDAR (Mizuno *et al.*, 2003; Xu *et al.*, 2006). As shown on Fig. 5A, expression of Fyn and Src and their respective phosphorylation at Y530 and Y416 were found similar between WT and THY-Tau22 mice (Fig. 5A). However, while Fyn distribution between sarkosyl-soluble and sarkosyl-insoluble fractions remained similar in WT and THY-Tau22 mice, the latter displayed a significant shift of Src from the sarkosyl-soluble to the sarkosyl-insoluble fraction containing pathological Tau species (insoluble/soluble ratio: +193.0 ± 16.6% in THY-Tau22 vs. WT, P = 0.005; n = 3 per group; Fig. 5B). Moreover, we observed that Src co-immunoprecipitated with total human Tau in the hippocampus of THY-Tau22 mice (Fig. 5C). Finally, we interestingly evidenced a shift of pY1472-NR2B and NR2B – but not NR2A – from the sarkosyl-soluble to the sarkosyl-insoluble fraction in THY-Tau22 mice as compared with WT animals (pY1472-NR2B: insoluble/soluble ratio: +513.3 ± 183.5% in THY-Tau22 vs. WT, P = 0.09; n = 3 per group; NR2B: insoluble/soluble ratio: +238.9 ± 30.5% in THY-Tau22 vs. WT, P = 0.0427; n = 3–4 per group; Fig. 6A). In line, NR2B co-immunoprecipitated with total human Tau, while NR2A did not (n = 3; Fig. 6B), suggestive of a protein interaction between NR2B and human Tau in the hippocampus of Tau transgenic mice.

Altogether, our data suggest that defective synaptic response to BDNF found in THY-Tau22 mice is independent from impaired TrkB/NMDAR crosstalk. Instead, our data suggest it is related to decreased NMDAR activatability ascribed to reduced phosphorylation at Y1472 through abnormal interaction of Src and NR2B with Tau and their mislocalization to insoluble protein fraction.

Discussion

Understanding the relationships between Tau pathology and memory impairments occurring with aging and in AD is a critical issue. The correlation between the spatiotemporal distribution of NFT and cognitive decline (Duyckaerts *et al.*, 1997) strongly suggests that Tau pathology plays an instrumental role in this decline. This is further substantiated by the observation of memory and long-term synaptic plasticity defects in several models of Tauopathies (Hoover *et al.*, 2010; Van der Jeugd *et al.*, 2011). The present study provides new insights into how Tau pathology may impair synaptic plasticity and specifically constitutes the first evidence of a defect of BDNF-promoted synaptic activity. Our data support this defect occurs as a consequence of NMDAR dysfunction.

Our experiments strengthen previous findings showing that at high rate of perfusion, BDNF readily induces enhancement of basal synaptic transmission in slices from adult mice through activation of TrkB and NMDAR (Diogenes *et al.*, 2007; Tebano *et al.*, 2008; Ji *et al.*, 2010). In line with previous data (for review see Blum & Konnerth, 2005), our electrophysiological observations indicated that such synaptic enhancement promoted by TrkB activation involves NR2B subunits. Noteworthy, this paradigm is based on exogenous BDNF application and cannot allow unraveling the role of endogenous BDNF on hippocampal synaptic transmission, which will deserve further evaluation.

The main finding of the present report is the significant attenuation of exogenous BDNF-induced synaptic enhancement of basal transmission in Tau transgenic mice. This occurred at a pathological stage at which neither overt neuronal death nor loss of hippocampal synaptic markers in the hippocampus had been described (Van der Jeugd *et al.*, 2011). Functional and structural integrity of THY-Tau22 hippocampal synapses was indicated here by the lack of significant changes in, respectively, the I/O curve and PSD95 and Syntaxin1 expressions in PSD and non-PSD fractions as compared with WT mice. The loss of BDNF effect upon basal synaptic transmission in THY-Tau22 mice is thus likely to be ascribed to functional changes rather than neurodegeneration and, as such, could be considered as an early defect promoted by Tau pathology that could take place during aging or in prodromal phases of AD.

Our biochemical data underlined that the lack of BDNF-induced synaptic enhancement in THY-Tau22 mice was unlikely related to reduced hippocampal TrkB expression and function. We particularly observed that the *in vivo* activatability of TrkB by either BDNF or Fluoxetine was not defective in THY-Tau22 mice. Rather, in steady-state conditions, we observed an increased hippocampal TrkB phosphorylation in THY-Tau22 mice compared with WT littermates, suggestive of an increased basal activation of the receptor. This might be the consequence of the significant increase in hippocampal BDNF levels we previously observed in our THY-Tau22 mice (Burnouf *et al.*, 2012). Moreover, Tau mice exhibited an enhanced TrkB response to BDNF. This may rely on either change of TrkB translocation to lipid rafts and/or change of TrkB trafficking. Translocation of TrkB receptors to lipid rafts is part of TrkB response to BDNF and is regulated by BDNF itself (Suzuki *et al.*, 2004), suggesting that increased basal levels of endogenous BDNF found in Tau mice (Burnouf *et al.*, 2012) could prime an increased translocation of TrkB to rafts thereby favoring later activation by exogenous BDNF. However, TrkB levels in hippocampal lipid rafts remained unchanged in Tau mice as were expression of A_{2A} receptors and Fyn kinase, both involved in TrkB translocation to lipid rafts (Pereira & Chao, 2007; Assaife-Lopes *et al.*, 2010). It remains, however, possible that increased TrkB response to BDNF may rely on trafficking changes. Indeed, upon neurotrophin binding, TrkB receptors are rapidly endocytosed (Zheng *et al.*, 2008), and some data support that internalized phosphorylated TrkB can mediate intraneuronal signaling (Zheng *et al.*, 2008; Spencer-Segal *et al.*, 2011 and references therein). Therefore, we cannot rule out that Tau pathology alters TrkB trafficking leading, *in fine*, to impaired BDNF-dependent synaptic enhancement observed in Tau mice. This will deserve further investigation.

It is noteworthy that BDNF application, while leading to synaptic potentiation in WT slices through activation of TrkB, induced a slight but significant decrease in synaptic activity in THY-Tau22 hippocampal slices. BDNF can also bind p75 receptor (Rodriguez-Tébar *et al.*, 1990). Interestingly, p75 expression is increased in NFT-bearing hippocampal

© 2012 The Authors
Aging Cell © 2012 Blackwell Publishing Ltd/Anatomical Society of Great Britain and Ireland

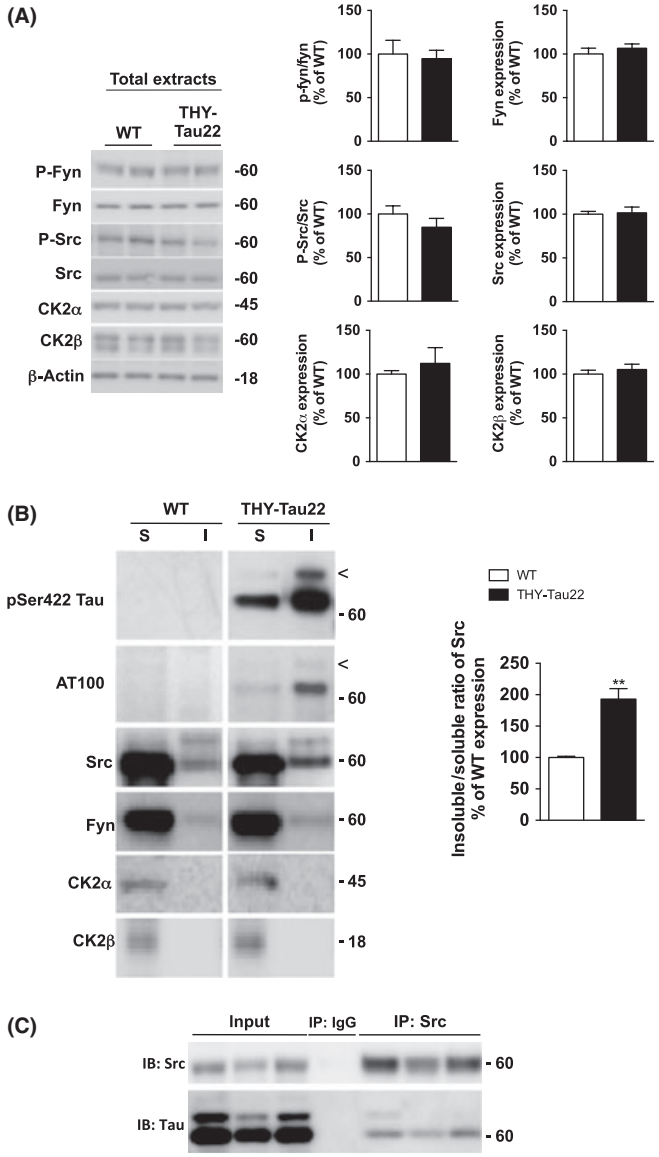

Fig. 5 Status of NR2B kinases in the hippocampus of THY-Tau22 mice. (A) Expression and phosphorylation of NR2B kinases in total protein extracts from 7-mo THY-Tau22 mice and littermate WT animals. Quantifications are given on the right panel. (B) Representative western blots of the levels of pathological Tau species (pSer422 and AT100), Src, Fyn, and CK2 subunits in sarkosyl-soluble (S) and sarkosyl-insoluble (I) protein fractions from the hippocampus of 7-mo WT and THY-Tau22 mice. Most hyperphosphorylated and insoluble forms of Tau are recovered within the sarkosyl-insoluble protein fraction in THY-Tau22 mice. This insoluble fraction displays increased levels of Src – but not Fyn – in THY-Tau22 mice as compared with WT mice. Right Panel: representative histogram of the ratio between sarkosyl-insoluble and sarkosyl-soluble Src proteins showing an increase in the hippocampus of THY-Tau22 mice. $n = 3$ per group. $^{**}P < 0.01$ vs. WT. (C) Src was immunoprecipitated and subsequent western blot (IP: Src, IB Tau) showed the presence of a Src-tau complex in the hippocampus of 7-mo THY-Tau22 mice. Immunoprecipitation with IgG-Beads (IP:IgG) constitutes a negative control. Biological replicates are represented on the blot. $n = 3$.

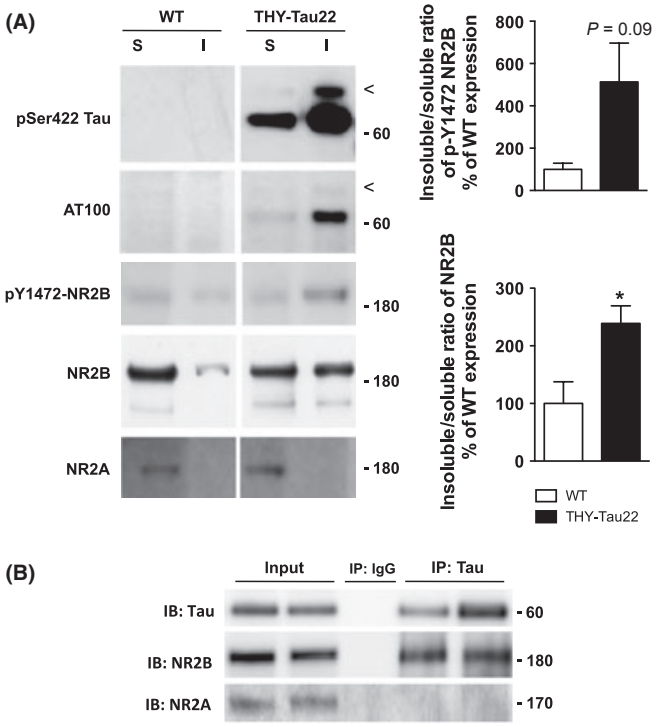

Fig. 6 Impaired NR2B distribution and interaction with human Tau in the hippocampus of THY-Tau22 mice. (A) Representative western blots of the levels of pathological Tau species (pSer422 and AT100), NR2B as well as NR2A subunits of the NMDAR in sarkosyl-soluble (S) and sarkosyl-insoluble (I) protein fractions from the hippocampus of 7-mo WT and THY-Tau22 mice. Most hyperphosphorylated and insoluble forms of Tau are recovered within the sarkosyl-insoluble protein fraction in THY-Tau22 mice. This insoluble fraction displays increased levels of Y1472 NR2B and NR2B subunits – but not NR2A – in THY-Tau22 mice as compared with WT mice. Right panel, representative histogram of the ratio between sarkosyl-insoluble and sarkosyl-soluble NR2B proteins showing an increase in the hippocampus of THY-Tau22 mice. $n = 3$–4 per group. $^{*}P < 0.05$ vs. WT. (B) Total human Tau was immunoprecipitated using the Tau5 antibody and subsequent western blot showed the pull-down of Tau (IB: total Tau) and of NR2B (IB: NR2B) in the hippocampus of 7-mo THY-Tau22 mice. Conversely, NR2A did not co-immunoprecipitate with Tau. Input is shown as a loading control. Immunoprecipitation with IgG-Beads (IP: IgG) constitutes a negative control. Biological replicates are represented on the blot. $n = 3$.

neurons of AD patients (Hu *et al.*, 2002) and in hippocampal membranes from a triple-transgenic mouse model of AD (Chakravarthy *et al.*, 2010). Puzzlingly, we observed a significant increase in p75 mRNA levels in THY-Tau22 mice hippocampus while the global protein amount remained unchanged. Interestingly, previous ultrastructural analysis suggested that most hippocampal p75 immunoreactivity is located primarily presynaptically in axons and terminals (Dougherty & Milner, 1999) raising the possibility that increased p75 mRNA levels reflect upregulation specifically in postsynaptic CA1 projection neurons. Upregulated p75 protein levels at the CA1 postsynaptic level might be diluted by using western blot on hippocampal total lysates. As p75 is known to be involved in synaptic depression (Woo *et al.*, 2005; Martinowich *et al.*, 2012), our results indicate that the transient fEPSP decrease following BDNF application we observed in Tau mice may be related to either unmasking of p75 effect on fEPSP due to the lack of the BDNF-induced synaptic enhancement and/or to postsynaptic p75 upregulation in CA1 neurons of THY-Tau22 mice. This point will deserve further investigation.

Strikingly, we observed a significant reduction of NMDA-induced basal synaptic depression in THY-Tau22 mice. These observations are in line with recent *in vitro* reports indicating that mutated Tau mislocalization to dendritic spines impairs NMDAR function (Hoover *et al.*, 2010). As synaptic enhancement promoted by BDNF is dependent on NMDAR and particularly on NR2B subunit, these data

© 2012 The Authors
Aging Cell © 2012 Blackwell Publishing Ltd/Anatomical Society of Great Britain and Ireland

support that impaired NMDAR function is determinant in the defective synaptic response to BDNF observed in Tau mice. This hypothesis is substantiated by our biochemical observations indicating, in THY-Tau22 mice, both reduced Y1472-NR2B phosphorylation and abnormal interaction of NR2B with Tau. Previous work indicated that Y1472-NR2B phosphorylation modulates NMDAR function and is critical for memory formation (Mizuno *et al.*, 2003; Barki-Harrington *et al.*, 2009). Its reduction in Tau mice might thus be related to memory impairments seen using the MWM task. Both Fyn and Src nonreceptor tyrosine kinases are known to directly phosphorylate NR2B at Y1472 (Prybylowski *et al.*, 2005; Zhang *et al.*, 2008; Sinai *et al.*, 2010). Effect of Fyn on NR2B has been recently shown to depend on normal Tau function (Ittner *et al.*, 2010). Our results indicate that neither expression nor phosphorylation of Fyn and Src were altered in Tau transgenic mice. However, while Fyn was mainly found in sarkosyl-soluble fractions, part of Src was mislocalized to sarkosyl-insoluble protein fractions of Tau transgenic mice, a phenomenon previously described in protein fractions from AD brains (Ho *et al.*, 2005). In addition, co-immunoprecipitation data indicated association of Src with human Tau in THY-Tau22 mice hippocampus. Other indirect mechanisms mediated by either CK2 or cdk5 may also regulate phosphorylation of NR2B at Y1472 (Zhang *et al.*, 2008; Sanz-Clemente *et al.*, 2010). However, neither CK2 expression/distribution nor NR2B phosphorylation at Ser1480 were changed in THY-Tau22 mice. Further, expression and distribution of cdk5 and co-activator p35 remained similar to controls (not shown). Altogether, our data support that reduced NR2B phosphorylation at Y1472 in Tau mice rely on Src loss-of-function due to a trapping by abnormal Tau species. Finally, besides reduced Y1472 phosphorylation, our data also suggest that abnormal Tau species directly impair NR2B function. Indeed, in THY-Tau22 mice, NR2B, but not NR2A, was shifted from the sarkosyl-soluble to the sarkosyl-insoluble protein fraction, which is rich in hyperphosphorylated and insoluble Tau species. This is in line with our co-immunoprecipitation data indicating that NR2B, but not NR2A, can be found associated with Tau protein in the hippocampus of THY-Tau22 mice.

Several studies support that BDNF can modulate NMDAR channel opening through a functional coupling between TrkB and NR2B subunits (Crozier *et al.*, 1999; and references herein), itself dependent on Fyn, but not Src (Mizuno *et al.*, 2003; Xu *et al.*, 2006). Such defective TrkB-NMDAR crosstalk could also promote impaired synaptic response to BDNF. However, the lack of Fyn impairment goes against this possibility. Abnormal Tau species may also interfere with other components involved in the functional coupling between TrkB and NMDAR. Previous data indicate that the ability of BDNF to enhance synaptic efficacy in a NMDAR-dependent manner can also be dependent on PLCγ (Garraway *et al.*, 2003). Our data do not support PLCγ impairments in the hippocampus of THY-Tau22 mice. Indeed, we did not observe any change in PLCγ phosphorylation nor expression in the hippocampus of Tau transgenic mice. Further, even if this signaling protein can interact with Tau in its N-terminal region (Reynolds *et al.*, 2008; Sergeant *et al.*, 2008 for review), solubility of PLCγ remained unaltered in the presence of insoluble pathological Tau species. Finally, BDNF-induced fEPSP enhancement in adult hippocampus has been particularly shown dependent on adenosine A_{2A} receptor function (Diogenes *et al.*, 2007; Tebano *et al.*, 2008). However, A_{2A} receptor expression and function remained unchanged in the hippocampus of THY-Tau22 mice (Fig. S4). All in all, our data suggest that lack of BDNF-mediated synaptic enhancement in THY-Tau22 mice is due to titration of both the NR2B kinase Src and NR2B itself, ultimately resulting in impaired Y1472 NR2B phosphorylation and function.

In conclusion, the present work thus unravels a new form of synaptic dysfunction promoted by Tau pathology. As NMDAR-dependent response to BDNF has been previously suggested to be involved in memory consolidation (Mizuno *et al.*, 2003), its impairment by pathological Tau species could be part of the process leading to memory impairments in these transgenic mice. Finally, together with other recent data (Hoover *et al.*, 2010; Brouillette *et al.*, 2012), our data support NMDAR as a convergent target functionally impaired by both Tau and amyloid pathologies that could play a substantial role in AD pathophysiology.

Materials and methods

Animals

Male THY-Tau22 mice and littermate controls (WT) animals of C57Bl6/J background were generated by overexpression of human 4-repeat Tau mutated at sites G272V and P301S under the control of Thy1.2 promoter (Schindowski *et al.*, 2006). Mice were housed in a pathogen-free facility, 5 per cage (Techniplast cages 1284L), with *ad libitum* access to food and water and maintained on a 12 h light:12 h dark cycle. Protocols were approved by the ethics committee of Nord-Pas-de-Calais following European regulations for animal welfare (Approval no. AF 06/2010, March 31, 2010).

Drugs and antibodies

K252a, MK801, CGS21680, and CHPG were obtained from Tocris (Milano, Italy). NMDA, Ifenprodil, BDNF, and fluoxetine-hydrochloride (FLX-HCl) were from Sigma-Aldrich (L'Isle d'Abeau, France). When used in slice electrophysiology experiments, pharmacological agents were diluted directly in the superfusion medium from stock solutions prepared in distilled water or dimethylsulfoxide (DMSO). The following antibodies were used in biochemical analysis: pSer212/pThr214 Tau (AT100, 1/1000; Thermo Scientific, Illkirch, France), pSer422 Tau (AP422, 1/2000; Biosource, Life Technologies, Saint-Aubin, France), pThr181 Tau (AT270, 1/5000; Pierce, Illkirch, France), total Tau (1/10 000; Tau Cter), PSD95 (Cell signaling, Saint-Quentin, France; 1/1000), Syntaxin1 (1/4000; Sigma-Aldrich), TrkB full-length (TrkB-FL, 1/1000; BD Bioscience, Le Pont de Claix, France), TrkB-T1 (1/1000; Santa Cruz, Heidelberg, Germany), pY705 TrkB (1/1000; Abcam, Paris, France), PLCγ (1/1000; CS), pY783 PLC (1/1000; CS), NR1 (1/500; Santa Cruz), NR2A (1/1000; CS), pY1472 NR2B (1/1000; CS), pS1480 NR2B (1/1000; Thermo Scientific), NR2B (1/1000; CS), CK2α (1/1000; CS); CK2β (1/1000; Sigma-Aldrich); Fyn (1/1000; CS); pY530 Fyn (1/1000; Abcam); Src (1/1000; CS); pY416 Src (1:1000; CS); p75 (1/1000; Millipore Billerica, MA, USA); β-actin (1/20 000; Sigma); and GAPDH (1/10 000; Santa Cruz).

Slice preparation and electrophysiology

Hippocampal slices from 7-mo THY-Tau22 mice or control WT mice were prepared as follows. After sacrifice, the hippocampus was removed and 450-μm slices cut with a McIlwain tissue slicer. Slices were maintained at room temperature (22–24°C) in artificial cerebrospinal fluid (ACSF) containing (in mM): 126 NaCl, 3.5 KCl, 1.2 NaH_2PO_4, 1.2 $MgCl_2$, 2 $CaCl_2$, 25 $NaHCO_3$, 11 glucose (pH 7.3) saturated with 95% O_2 and 5% CO_2. After incubation in ACSF for at least 1 h, a single slice was transferred to a submerged recording chamber and continuously superfused at 32–33°C with ACSF at a rate of 2.6 mL min^{-1}. The drugs

© 2012 The Authors
Aging Cell © 2012 Blackwell Publishing Ltd/Anatomical Society of Great Britain and Ireland

were added to this superfusion medium. The perfusion apparatus was made of chemically inert materials (i.e., silicone tubing). Recordings were made with a glass pipette containing 2 mol L^{-1} NaCl (2–5 MΩ), placed in stratum radiatum. Stimuli were delivered to Schaffer collaterals through an insulated bipolar twisted NiCr electrode (50 μm OD) every 20 s (square pulses of 100 μs duration at a frequency of 0.05 Hz), and three consecutive responses were averaged. The stimulation intensity used in the fEPSP recordings was in the 36–60 μA range and was always adjusted to obtain a submaximal fEPSP slope (~60% of maximum) with minimum population spike contamination. Signals were acquired with a DAM-80 AC differential amplifier (WPI) and analyzed with the LTP program (Anderson & Collingridge, 2001). At least 10 min of stable baseline recording preceded drug application. Data were expressed as mean ± SEM of n experiments (one slice tested per experiment. Slices were obtained from at least two animals for each set of experiment). To allow for comparisons between different experiments, slope values were normalized, taking the average of the baseline values to be 100%. The drug effect was expressed as the mean percentage variation of the slope from baseline over the last 5 min of drug perfusion. The washout period lasted at least 30 min.

Input/output (I/O) plots

For each slice, single stimuli were delivered every 20 s (square pulses of 100 μs duration at a frequency of 0.05 Hz), and three consecutive responses were averaged. Once the response was stable, the minimum stimulus intensity necessary to evoke an observable response was measured. An I/O curve was then obtained by recording averaged responses at ~4 μA increments, starting at the threshold stimulation intensity (~30 μA) and ending with a *plateau* at a maximum of ~56 μA. Each point on the I/O curve was obtained by averaging responses over at least 5 min of recording. The I/O curves were plotted as the relationship of fEPSP slope vs. fiber volley amplitude, which provides a measure of synaptic efficiency.

Biochemical analysis

Total protein extracts were prepared as follows: tissue was directly sonicated in a buffer containing 0.32 M sucrose and 10 mM Tris–HCl, pH 7.4. Crude homogenates were directly mixed with 2× reducing LDS Sample Buffer (Life Technologies, Saint-Aubin, France) and heated at 100°C for 10 min.

Postsynaptic density fractions were obtained based on the protocol described by (Milnerwood *et al.*, 2010). Briefly, hippocampi were homogenized in 500-μL cold buffer containing 0.32 M sucrose and 10 mM HEPES, pH 7.4. Homogenates were cleared twice at 1000 ***g*** for 10 min to remove nuclei and large debris. The resulting supernatants were centrifuged at 12 000 ***g*** for 20 min, after which the pellets were washed twice in a HEPES (4 mM)-EDTA (1 mM) solution at pH 7.4. Then, the pellets were incubated for 15 min at 4°C in 20 mM HEPES, 100 mM NaCl, 0.5% Triton X-100, pH 7.2 and subsequently centrifuged at 12 000 ***g*** for 20 min. The resulting supernatants were considered as the non-postsynaptic density (non-PSD) fraction, as confirmed by the detection of enriched Syntaxin1 and sparse PSD95 by western blotting (see Fig. 2B, lower panel). The pellet was solubilized for 1 h at 4°C in 20 mM HEPES, 150 mM NaCl, 1% Triton X-100, 1% sodium deoxycholate, 1% SDS, pH 7.5 and then centrifuged at 10 000 ***g*** for 15 min. The resulting supernatants contained the postsynaptic density (PSD) fraction, as shown through enriched PSD95 and sparse Syntaxin1 contents (Fig. 2B, lower panel).

For sarkosyl-soluble/insoluble protein preparations, hippocampi were homogenized by sonication in a lysis buffer containing 10 mM Tris–HCl pH 7.4, 0.32 M sucrose, 800 mM NaCl, 1 mM EGTA with protease inhibitors (Complete w/o EDTA, Roche) and centrifuged at 12 000 g for 10 min at 4°C, and the resulting supernatants centrifuged at 100 000 ***g*** for 1 h at 4°C. The resulting pellets were then homogenized for 1 h at room temperature in 400 μL of lysis buffer supplemented with 1% N-lauryl sarcosine sodium salt and centrifuged at 100 000 ***g*** for 1 h at 4°C. Final supernatants and pellets corresponded to sarkosyl-soluble and insoluble fractions, respectively. Sarkosyl-soluble proteins were quantified using the BCA assay, and sarkosyl-insoluble proteins directly resuspended in 100-μL LDS 2× supplemented with reducing agents (Invitrogen, Saint-Aubin, France). For western blot analysis, 2 μg of sarkosyl-soluble proteins and a 1:2 v/v suspension of sarkosyl-insoluble proteins were loaded onto NuPage Novex gels.

In the different biochemical experiments performed, protein amounts were evaluated using the BCA assay (Pierce), subsequently diluted with LDS 2× supplemented with reducing agents (Invitrogen), and then separated on NuPage Novex gels (Invitrogen). Proteins were transferred to nitrocellulose membranes, which were then saturated with 5% nonfat dry milk in TNT (Tris 15 mM pH8, NaCl 140 mM, 0.05% Tween) and incubated with primary and secondary antibodies. Signals were visualized using chemiluminescence kits (ECL™; Amersham Bioscience, Templemars, France) and Hyperfilms (GE Healthcare, Templemars, France). Results were normalized to GAPDH or β-actin, and quantification was performed using ImageJ software (Scion Software).

TrkB immunoprecipitation

TrkB activation was assessed by evaluating Y705 phosphorylation using a pY705-TrkB antibody (Abcam; 1/1000), following a lectin-affinity precipitation, as previously described (Rantamaki *et al.*, 2007). Briefly, hippocampi were homogenized with glass/teflon potter in 400-μL ice-cold lysis buffer containing 137 mM NaCl, 20 mM Tris–HCl pH 8, 1% NP40, 10% glycerol, protease inhibitor (Complete w/o EDTA, Roche, La Rochelle, France) and 1 mM sodium orthovanadate, kept 15 min on ice and centrifuged at 16 100 ***g*** during 15 min. Supernatant protein levels were quantified using BCA system. 500 μg of hippocampal proteins were incubated with 15 μL of ConA Sepharose™ lectin (GE Healthcare, Templemars, France) during 2 h at 4°C. Following centrifugation, supernatants were removed, and the lectin beads were washed twice with lysis buffer. 20 μL of LDS supplemented with reducing agents were added to the beads and heated at 100°C for 10 min. Then, supernatants were quickly removed after centrifugation and loaded on NuPage Novex gels for western Blot analysis.

Co-immunoprecipitation procedure

For co-immunoprecipitation studies, Tris–sucrose hippocampal homogenates were dissolved in ice-cold lysis buffer (50 mM Tris–HCl pH 7.4, 150 mM NaCl, 1 mM EDTA, 1% Nonidet P-40, 0.5% Na-Deoxycholate) supplemented with protease inhibitors (Complete Mini, Roche). The lysates were sonicated, homogenized during 1 h at 4°C, and then centrifuged at 12 000 ***g*** during 20 min at 4°C. Supernatant protein levels were quantified using the BCA system. 200 μL of protein lysates (1 mg mL^{-1}) were incubated with the IP antibody (Tau5, 1/10, Invitrogen or Src, 1/100, CS) during 1 h at 4°C with gentle rocking and then incubated overnight at 4°C with 20 μL of anti-mouse or rabbit-IgG TrueBlot™ beads. Samples were then microcentrifuged at 2000 ***g*** at 4°C for 5 min, and the pellets were washed 3 times in

© 2012 The Authors
Aging Cell © 2012 Blackwell Publishing Ltd/Anatomical Society of Great Britain and Ireland

ice-cold lysis buffer. Immunoprecipitates were resuspended in 2× LDS buffer supplemented with NuPAGE reducing agents and boiled for 10 min before gel loading and western blot analysis. Control experiments using IgG TrueBlot™ beads without IP antibody were performed in the same way as samples.

Immunohistochemistry

Immunohistochemical detection of abnormally phosphorylated Tau species (pSer212/pThr214), visualized with diaminobenzidine (DAB), was performed as previously described using the AT100 antibody (1/400; TS) (Schindowski *et al.*, 2006).

In vivo TrkB activation

FLX-HCl was diluted in 0.9% NaCl at a concentration of 3 mg mL^{-1} and injected intraperitoneally (30 mg kg^{-1}). Control animals were injected with equivalent volumes of 0.9% NaCl. Mice were killed 60 min following injection. For stereotaxic injections, 100 ng of human recombinant BDNF were diluted in 2 μL PBS and injected into the CA1 region of the hippocampus (coordinates from Bregma: −2.8 mm posterior, −2.0 mm lateral, −1.5 mm below the brain surface) at a rate of 0.25 μL min^{-1}. Mice were killed 10 min after the end of injection. In both cases, brains were rapidly removed, and the hippocampi dissected out and stored at −80°C for further biochemical analyses.

Lipid rafts

Hippocampi were homogenized with 500-μL ice-cold TBST buffer (10 mM Trizma Base pH 8, 150 mM NaCl, 1% Triton X-100, protease inhibitor (Complete w/o EDTA), 125 nM okadaic acid and 1 mM sodium orthovanadate) using a glass/teflon potter, kept on ice for 30 min and centrifuged at 1000 ***g*** for 10 min. Supernatant protein levels were quantified using the BCA system. Hippocampal proteins (1000 μg) were loaded at the bottom of a discontinuous sucrose gradient by mixing 350 μL of sample with 350 μL of 85% sucrose TBST solution in SW41 centrifuge tubes (Beckman). The resulting 42.5% sucrose solutions were sequentially covered with 6 mL of 35% sucrose TBST solution and 1.3 mL of 5% sucrose TBST solution. Protease and phosphatase inhibitors were present in all layers. The tubes were spun at 200 000 g for 18 h at 4°C in a Beckman Optima-XL centrifuge using an SW41 rotor. Eight fractions of 1 mL each were then collected from the top. Each fraction was sonicated. Fraction 2 was identified as the lipid raft fraction by Dot Blot analysis using the GM1 marker (Fig. S2). Concerning Dot Blot, 1 μL of each fraction was loaded onto a nitrocellulose membrane, followed by saturation with 5% nonfat dry milk in TNT and incubation with HRP-conjugated Cholera Toxin Subunit (1/1000; Sigma). For TrkB detection, each fraction was concentrated by a methanol-chloroform precipitation. Total cholesterol was dosed in lipid raft fraction 2 by the enzymatic method using ready-to-use kits (Biomérieux, Craponne, France).

Morris water maze task

Spatial learning and memory abilities were examined in a standard hidden-platform acquisition and retention version of the Morris water maze task (Van der Jeugd *et al.*, 2011). A 90-cm circular pool was filled with water opacified with nontoxic white paint and kept at 21°C and a 10-cm round rescue platform was hidden 1 cm beneath the surface of the water at a fixed position. Four positions around the edge of the tank were arbitrarily designated in order to divide it into four equal quadrants (clockwise): target (which contains the rescue platform), adjacent1, opposite, and adjacent2. Each mouse was given four swimming trials per day with at least 10 min of intertrial interval, for four consecutive training days. The start position was pseudo-randomized across trials. Mice that failed to find the submerged rescue platform within 2 min were guided to it and were allowed to remain on it for 15 s before going back to their cages. The time required to find the hidden rescue platform (escape latency) was used as a spatial learning index and was recorded using the Ethovision XT video tracking system (Noldus Information Technology, Paris, France). Swimming speed (i.e., velocity) was also measured to rule out any possible motor defect that could interfere with the ability to perform in this task. 24 h after the acquisition phase, spatial memory was evaluated in a 60 s probe trial during which the rescue platform was removed. The proportion of time spent in the target quadrant vs. the other targets was considered as a spatial memory index.

mRNA extraction and quantitative real-time RT-PCR analysis

Total RNA was extracted from hippocampi and purified using the RNeasy Lipid Tissue Mini Kit (Qiagen, Courtaboeuf, France). One microgram of total RNA was reverse transcribed using the Applied Biosystems High-Capacity cDNA reverse transcription kit. Quantitative real-time RT-PCR analysis was performed on an Applied Biosystems Prism 7900 System using Power SYBR Green PCR Master Mix. The thermal cycler conditions were as follows: hold for 10 min at 95°C, followed by 45 cycles of a two-step PCR consisting of a 95°C step for 15 s followed by a 60°C step for 25 s. Primer sequences used are as follows: 5′-ggctgtgaagacgctgaagg-3′ (TrkB-FL forward), 5′-ttgacaatgtgctcgtgctg-3′ (TrkB-FL reverse), 5′-actgagcgc-cagttacgc-3′ (p75 forward), 5′-cgtagaccttgtgatccatcg-3′ (p75 reverse), 5′-cgtacggggatgaccaacgc-3′ (NR2A forward), 3′-ctgtggccccgactgtccct-5′ (NR2A reverse), 5′-gggttacaaccggtgccta-3′ (NR2B forward), 5′-ctttgcc-gatggtgaaagat-3′ (NR2B reverse), 5′-agcatacaggtcctggcatc-3′ (cyclophilin A forward), 5′-ttcaccttcccaaagaccac-3′ (cyclophilin A reverse). Cyclophilin A was used as internal control. Amplifications were carried out in triplicate, and the relative expression of target genes was determined by the ΔΔCT method.

Statistics

Results are expressed as means ± SEM. Statistical analyses were performed using the Mann–Whitney *U*-test software, Student's t-test or Two-Way ANOVA when appropriated using Graphpad Prism. A *P*-value of <0.05 was considered to indicate a significant difference.

Acknowledgments

This work has been developed and supported in part through Inserm, CNRS, DN2M, FEDER, France Alzheimer, IMPRT, University of Lille 2, Lille Regional Hospital (CHRU), Région Nord/Pas-de-Calais, Fondation Cœur and Artères, LECMA, MEDIALZ and ANR (AMYTOXTAU and ADONTAGE grants), the European Community (MEMOSAD; FP7 contract 200611), MEDIALZ and the LABEX (excellence laboratory, program invest for the future) DISTALZ (Development of Innovative Strategies for a Transdisciplinary approach to ALZheimer's disease), PhD students were recipients of scholarships from Région Nord/Pas-de-Calais as well as CHRU (KB, SB, MD) and University of Lille 2/French Research Ministry (LT, CL, AL). FJFG is supported by a fellowship from the Communidad Castilla-La-Mancha. We would like to thank Dr. Rantamaki and Dr. Castren for the TrkB lectin precipitation protocol. We acknowledge Georges Grard for his help for setting up lipid raft experiments, and Ingrid Brion and Bérangère Barbot for mouse care

© 2012 The Authors
Aging Cell © 2012 Blackwell Publishing Ltd/Anatomical Society of Great Britain and Ireland

and genotyping. Manuscript editing assistance was provided by S. Rasika of Gap Junction. Authors have no conflict of interest regarding this work.

Author contributions

SB, AM, PP, LB, and DB designed and made experiments, analyzed the results and wrote the manuscript. AB, NS, MH, and SH designed experiments and wrote the manuscript. MD, CL, KB, AL, FJFG, LT, SE, MEG, DD, and AMT made experiments.

References

Allaman I, Fiumelli H, Magistretti PJ, Martin JL (2011) Fluoxetine regulates the expression of neurotrophic/growth factors and glucose metabolism in astrocytes. *Psychopharmacology* **216**, 75–84.

Anderson WW, Collingridge GL (2001) The LTP Program: a data acquisition program for on-line analysis of long-term potentiation and other synaptic events. *J. Neurosci. Methods* **108**, 71–83.

Assaife-Lopes N, Sousa VC, Pereira DB, Ribeiro JA, Chao MV, Sebastião AM (2010) Activation of adenosine A2A receptors induces TrkB translocation and increases BDNF-mediated phospho-TrkB localization in lipid rafts: implications for neuromodulation. *J. Neurosci.* **30**, 468–480.

Ballatore C, Lee VM, Trojanowski JQ (2007) Tau-mediated neurodegeneration in Alzheimer's disease and related disorders. *Nat. Rev. Neurosci.* **8**, 663–672.

Barki-Harrington L, Elkobi A, Tzabary T, Rosenblum K (2009) Tyrosine phosphorylation of the 2B subunit of the NMDA receptor is necessary for taste memory formation. *J. Neurosci.* **29**, 9219–9226.

Belarbi K, Burnouf S, Fernandez-Gomez FJ, Laurent C, Lestavel S, Figeac M, Sultan A, Troquier L, Leboucher A, Caillierez R, Grosjean ME, Demeyer D, Obriot H, Brion I, Barbot B, Galas MC, Staels B, Humez S, Sergeant N, Schraen-Maschke S, Muhr-Tailleux A, Hamdane M, Buee L, Blum D (2011) Beneficial effects of exercise in a transgenic mouse model of Alzheimer's disease-like Tau pathology. *Neurobiol. Dis.* **43**, 486–494.

Blum R, Konnerth A (2005) Neurotrophin-mediated rapid signaling in the central nervous system: mechanisms and functions. *Physiology* **20**, 70–78.

Blurton-Jones M, Kitazawa M, Martinez-Coria H, Castello NA, Muller FJ, Loring JF, Yamasaki TR, Poon WW, Green KN, LaFerla FM (2009) Neural stem cells improve cognition via BDNF in a transgenic model of Alzheimer disease. *Proc. Natl Acad. Sci. USA* **106**, 13594–13599.

Braak H, Thal DR, Ghebremedhin E, Del Tredici K (2011) Stages of the pathologic process in Alzheimer disease: age categories from 1 to 100 years. *J. Neuropathol. Exp. Neurol.* **70**, 960–969.

Brouillette J, Caillierez R, Zommer N, Alves-Pires C, Benilova I, Blum D, De Strooper B, Buée L (2012) Neurotoxicity and memory deficits induced by soluble low-molecular-weight amyloid-β1-42 oligomers are revealed in vivo by using a novel animal model. *J. Neurosci.* **32**, 7852–7861.

Burnouf S, Belarbi K, Troquier L, Derisbourg M, Demeyer D, Leboucher A, Laurent C, Hamdane M, Buee L, Blum D (2012) Hippocampal BDNF expression in a Tau transgenic mouse model. *Curr. Alzheimer Res.* **9**, 406–410.

Chakravarthy B, Gaudet C, Ménard M, Atkinson T, Brown L, Laferla FM, Armato U, Whitfield J (2010) Amyloid-beta peptides stimulate the expression of the p75 (NTR) neurotrophin receptor in SHSY5Y human neuroblastoma cells and AD transgenic mice. *J Alzheimers Dis.* **19**, 915–925.

Cirulli F, Berry A, Chiarotti F, Alleva E (2004) Intrahippocampal administration of BDNF in adult rats affects short-term behavioral plasticity in the Morris water maze and performance in the elevated plus-maze. *Hippocampus* **14**, 802–807.

Crozier RA, Black IB, Plummer MR (1999) Blockade of NR2B-containing NMDA receptors prevents BDNF enhancement of glutamatergic transmission in hippocampal neurons. *Learn Mem.* **6**, 257–266.

Diogenes MJ, Assaife-Lopes N, Pinto-Duarte A, Ribeiro JA, Sebastiao AM (2007) Influence of age on BDNF modulation of hippocampal synaptic transmission: interplay with adenosine A2A receptors. *Hippocampus* **17**, 577–585.

Domenici MR, Pintor A, Potenza RL, Gaudi S, Gro MC, Passarelli F, Reggio R, Galluzzo M, Massotti M, Popoli P (2003) Metabotropic glutamate receptor 5 (mGluR5)-mediated phosphoinositide hydrolysis and NMDA-potentiating effects are blunted in the striatum of aged rats: a possible additional mechanism in striatal senescence. *Eur. J. Neurosci.* **17**, 2047–2055.

Dougherty KD, Milner TA (1999) p75NTR immunoreactivity in the rat dentate gyrus is mostly within presynaptic profiles but is also found in some astrocytic and postsynaptic profiles. *J Comp. Neurol.* **407**, 77–91.

Duyckaerts C, Bennecib M, Grignon Y, Uchihara T, He Y, Piette F, Hauw JJ (1997) Modeling the relation between neurofibrillary tangles and intellectual status. *Neurobiol. Aging* **18**, 267–273.

Garraway SM, Petruska JC, Mendell LM (2003) BDNF sensitizes the response of lamina II neurons to high threshold primary afferent inputs. *Eur. J. Neurosci.* **18**, 2467–2476.

Garzon DJ, Fahnestock M (2007) Oligomeric amyloid decreases basal levels of brain-derived neurotrophic factor (BDNF) mRNA via specific downregulation of BDNF transcripts IV and V in differentiated human neuroblastoma cells. *J. Neurosci.* **27**, 2628–2635.

Heldt SA, Stanek L, Chhatwal JP, Ressler KJ (2007) Hippocampus-specific deletion of BDNF in adult mice impairs spatial memory and extinction of aversive memories. *Mol. Psychiatry* **12**, 656–670.

Ho GJ, Hashimoto M, Adame A, Izu M, Alford MF, Thal LJ, Hansen LA, Masliah E (2005) Altered p59Fyn kinase expression accompanies disease progression in Alzheimer's disease: implications for its functional role. *Neurobiol. Aging* **26**, 625–635.

Hofer M, Pagliusi SR, Hohn A, Leibrock J, Barde YA (1990) Regional distribution of brain-derived neurotrophic factor mRNA in the adult mouse brain. *EMBO J.* **9**, 2459–2464.

Hoover BR, Reed MN, Su J, Penrod RD, Kotilinek LA, Grant MK, Pitstick R, Carlson GA, Lanier LM, Yuan LL, Ashe KH, Liao D (2010) Tau mislocalization to dendritic spines mediates synaptic dysfunction independently of neurodegeneration. *Neuron* **68**, 1067–1081.

Hu XY, Zhang HY, Qin S, Xu H, Swaab DF, Zhou JN (2002) Increased p75(NTR) expression in hippocampal neurons containing hyperphosphorylated tau in Alzheimer patients. *Exp. Neurol.* **178**, 104–111.

Ittner LM, Ke YD, Delerue F, Bi M, Gladbach A, van Eersel J, Wolfing H, Chieng BC, Christie MJ, Napier IA, Eckert A, Staufenbiel M, Hardeman E, Gotz J (2010) Dendritic function of tau mediates amyloid-beta toxicity in Alzheimer's disease mouse models. *Cell* **142**, 387–397.

Ji Y, Lu Y, Yang F, Shen W, Tang TT, Feng L, Duan S, Lu B (2010) Acute and gradual increases in BDNF concentration elicit distinct signaling and functions in neurons. *Nat. Neurosci.* **13**, 302–309.

Kesslak JP, So V, Choi J, Cotman CW, Gomez-Pinilla F (1998) Learning upregulates brain-derived neurotrophic factor messenger ribonucleic acid: a mechanism to facilitate encoding and circuit maintenance? *Behav. Neurosci.* **112**, 1012–1019.

Mallon AP, Auberson YP, Stone TW (2005) Selective subunit antagonists suggest an inhibitory relationship between NR2B and NR2A-subunit containing N-methyl-D: -aspartate receptors in hippocampal slices. *Exp. Brain Res.* **162**, 374–383.

Martinowich K, Schloesser RJ, Lu Y, Jimenez DV, Paredes D, Greene JS, Greig NH, Manji HK, Lu B (2012) Roles of p75(NTR), long-term depression, and cholinergic transmission in anxiety and acute stress coping. *Biol. Psychiatry* **71**, 75–83.

Masters CL, Simms G, Weinman NA, Multhaup G, McDonald BL, Beyreuther K (1985) Amyloid plaque core protein in Alzheimer disease and Down syndrome. *Proc. Natl Acad. Sci. USA* **82**, 4245–4249.

Milnerwood AJ, Gladding CM, Pouladi MA, Kaufman AM, Hines RM, Boyd JD, Ko RW, Vasuta OC, Graham RK, Hayden MR, Murphy TH, Raymond LA (2010) Early increase in extrasynaptic NMDA receptor signaling and expression contributes to phenotype onset in Huntington's disease mice. *Neuron* **65**, 178–190.

Minichiello L (2009) TrkB signalling pathways in LTP and learning. *Nat. Rev. Neurosci.* **10**, 850–860.

Minichiello L, Korte M, Wolfer D, Kuhn R, Unsicker K, Cestari V, Rossi-Arnaud C, Lipp HP, Bonhoeffer T, Klein R (1999) Essential role for TrkB receptors in hippocampus-mediated learning. *Neuron* **24**, 401–414.

Mizuno M, Yamada K, He J, Nakajima A, Nabeshima T (2003) Involvement of BDNF receptor TrkB in spatial memory formation. *Learn Mem.* **10**, 108–115.

Mu JS, Li WP, Yao ZB, Zhou XF (1999) Deprivation of endogenous brain-derived neurotrophic factor results in impairment of spatial learning and memory in adult rats. *Brain Res.* **835**, 259–265.

Nagahara AH, Merrill DA, Coppola G, Tsukada S, Schroeder BE, Shaked GM, Wang L, Blesch A, Kim A, Conner JM, Rockenstein E, Chao MV, Koo EH, Geschwind D, Masliah E, Chiba AA, Tuszynski MH (2009) Neuroprotective effects of brain-derived neurotrophic factor in rodent and primate models of Alzheimer's disease. *Nat. Med.* **15**, 331–337.

Peng S, Garzon DJ, Marchese M, Klein W, Ginsberg SD, Francis BM, Mount HT, Mufson EJ, Salehi A, Fahnestock M (2009) Decreased brain-derived neurotrophic factor depends on amyloid aggregation state in transgenic mouse models of Alzheimer's disease. *J. Neurosci.* **29**, 9321–9329.

Pereira DB, Chao MV (2007) The tyrosine kinase Fyn determines the localization of TrkB receptors in lipid rafts. *J. Neurosci.* **27**, 4859–4869.

Poon WW, Blurton-Jones M, Tu CH, Feinberg LM, Chabrier MA, Harris JW, Jeon NL, Cotman CW (2011) beta-Amyloid impairs axonal BDNF retrograde trafficking. *Neurobiol. Aging* **32**, 821–833.

© 2012 The Authors
Aging Cell © 2012 Blackwell Publishing Ltd/Anatomical Society of Great Britain and Ireland

Prybylowski K, Chang K, Sans N, Kan L, Vicini S, Wenthold RJ (2005) The synaptic localization of NR2B-containing NMDA receptors is controlled by interactions with PDZ proteins and AP-2. *Neuron*, **47**, 845–857.

Rantamaki T, Hendolin P, Kankaanpaa A, Mijatovic J, Piepponen P, Domenici E, Chao MV, Mannisto PT, Castren E (2007) Pharmacologically diverse antidepressants rapidly activate brain-derived neurotrophic factor receptor TrkB and induce phospholipase-Cgamma signaling pathways in mouse brain. *Neuropsychopharmacology* **32**, 2152–2162.

Reynolds CH, Garwood CJ, Wray S, Price C, Kellie S, Perera T, Zvelebil M, Yang A, Sheppard PW, Varndell IM, Hanger DP, Anderton BH (2008) Phosphorylation regulates tau interactions with Src homology 3 domains of phosphatidylinositol 3-kinase, phospholipase Cgamma1, Grb2, and Src family kinases. *J. Biol. Chem.* **283**, 18177–18186.

Rodriguez-Tébar A, Dechant G, Barde YA (1990) Binding of brain-derived neurotrophic factor to the nerve growth factor receptor. *Neuron* **4**, 487–492.

Sanz-Clemente A, Matta JA, Isaac JT, Roche KW (2010) Casein kinase 2 regulates the NR2 subunit composition of synaptic NMDA receptors. *Neuron* **67**, 984–996.

Schindowski K, Bretteville A, Leroy K, Begard S, Brion JP, Hamdane M, Buee L (2006) Alzheimer's disease-like tau neuropathology leads to memory deficits and loss of functional synapses in a novel mutated tau transgenic mouse without any motor deficits. *Am. J. Pathol.* **169**, 599–616.

Schindowski K, Belarbi K, Buee L (2008) Neurotrophic factors in Alzheimer's disease: role of axonal transport. *Genes Brain Behav.* **7**(Suppl 1), 43–56.

Sergeant N, Bretteville A, Hamdane M, Caillet-Boudin ML, Grognet P, Bombois S, Blum D, Delacourte A, Pasquier F, Vanmechelen E, Schraen-Maschke S, Buee L (2008) Biochemistry of Tau in Alzheimer's disease and related neurological disorders. *Expert Rev. Proteomics* **5**, 207–224.

Sinai L, Duffy S, Roder JC (2010) Src inhibition reduces NR2B surface expression and synaptic plasticity in the amygdala. *Learn Mem.* **17**, 364–371.

Spencer-Segal JL, Waters EM, Bath KG, Chao MV, McEwen BS, Milner TA (2011) Distribution of phosphorylated TrkB receptor in the mouse hippocampal formation depends on sex and estrous cycle stage. *J. Neurosci.* **31**, 6780–6790.

Suzuki S, Numakawa T, Shimazu K, Koshimizu H, Hara T, Hatanaka H, Mei L, Lu B, Kojima M (2004) BDNF-induced recruitment of TrkB receptor into neuronal lipid rafts: roles in synaptic modulation. *J. Cell Biol.* **167**, 1205–1215.

Tebano MT, Martire A, Rebola N, Pepponi R, Domenici MR, Gro MC, Schwarzschild MA, Chen JF, Cunha RA, Popoli P (2005) Adenosine A2A receptors and metabotropic glutamate 5 receptors are co-localized and functionally interact in the hippocampus: a possible key mechanism in the modulation of N-methyl-D-aspartate effects. *J. Neurochem.* **95**, 1188–1200.

Tebano MT, Martire A, Potenza RL, Gro C, Pepponi R, Armida M, Domenici MR, Schwarzschild MA, Chen JF, Popoli P (2008) Adenosine A(2A) receptors are required for normal BDNF levels and BDNF-induced potentiation of synaptic transmission in the mouse hippocampus. *J. Neurochem.* **104**, 279–286.

Van der Jeugd A, Ahmed T, Burnouf S, Belarbi K, Hamdame M, Grosjean ME, Humez S, Balschun D, Blum D, Buee L, D'Hooge R (2011) Hippocampal tauopathy in tau transgenic mice coincides with impaired hippocampus-dependent learning and memory, and attenuated late-phase long-term depression of synaptic transmission. *Neurobiol. Learn. Mem.* **95**, 296–304.

Woo NH, Teng HK, Siao CJ, Chiaruttini C, Pang PT, Milner TA, Hempstead BL, Lu B (2005) Activation of p75NTR by proBDNF facilitates hippocampal long-term depression. *Nat. Neurosci.* **8**, 1069–1077.

Xu F, Plummer MR, Len GW, Nakazawa T, Yamamoto T, Black IB, Wu K (2006) Brain-derived neurotrophic factor rapidly increases NMDA receptor channel activity through Fyn-mediated phosphorylation. *Brain Res.* **1121**, 22–34.

Zhang S, Edelmann L, Liu J, Crandall JE, Morabito MA (2008) Cdk5 regulates the phosphorylation of tyrosine 1472 NR2B and the surface expression of NMDA receptors. *J. Neurosci.* **28**, 415–424.

Zheng J, Shen WH, Lu TJ, Zhou Y, Chen Q, Wang Z, Xiang T, Zhu YC, Zhang C, Duan S, Xiong ZQ (2008) Clathrin-dependent endocytosis is required for TrkB-dependent Akt-mediated neuronal protection and dendritic growth. *J. Biol. Chem.* **283**, 13280–13288.

Zheng Z, Sabirzhanov B, Keifer J (2010) Oligomeric amyloid-{beta} inhibits the proteolytic conversion of brain-derived neurotrophic factor (BDNF), AMPA receptor trafficking, and classical conditioning. *J. Biol. Chem.* **285**, 34708–34717.

Supporting Information

Additional Supporting Information may be found in the online version of this article at the publisher's web-site.

Fig. S1 Hippocampal p75 expression in THY-Tau22 mice.

Fig. S2 Hippocampal lipid raft integrity in THY-Tau22 mice.

Fig. S3 Expression, phosphorylation, and distribution of PLCγ in THY-Tau22 mice.

Fig. S4 A_{2A} mRNA expression and A_{2A}R-dependent facilitation of mGlu5R effects.

© 2012 The Authors
Aging Cell © 2012 Blackwell Publishing Ltd/Anatomical Society of Great Britain and Ireland